Design, implementation and characterization of a BioMEMS testing device.

F Schaumburg[1], **M C Perez**[1,2], **Zalazar M A**[1], **F A Guarnieri**[1,2]
[1] Laboratorio de BioMEMS, Facultad de Ingeniería, Universidad Nacional de Entre Ríos, Ruta 11 Km 10,Oro Verde (3100), Entre Ríos, Argentina.
[2]Centro Internacional de Métodos Computacionales en Ingeniería (CIMEC), (INTEC-CONICET-UNL**),** Colectora Ruta Nacional 168 Km 472, Santa Fe, Argentina.

E-mail: schaumburg.f@gmail.com, mcperez78@gmail.com, martin.zalazar@fulbrightmail.org, aguarni@santafe-conicet.gov.ar

Abstract. Several issues have been reported regarding aqueous shunts used in the treatment of glaucoma. To attend to these problems an active implantable valve, based in MEMS (mirco electromecanic structure) processes, is proposed. This BioMEMS would be fed wirelessly and would be composed of an integrated circuit, an electrochemical actuator and microfuidics. In order to assess functionality and to optimize these blocks, it is desirable to test them prior to the development of the implant. In this paper a circuit for testing the energy source, the RF link, and the actuator of the active valve was developed and characterized.

1. Introduction

About 1% of world's population suffers from glaucoma, a disease of uncertain etiology. For that reason no cure was still developed and the available treatment options act over the main symptom: the elevated intra-ocular pressure. Those who suffer from this condition can choose among eye-drops, pills, and valves. Eye-drops are suitable during the first stages of glaucoma, but as the disease follows its course other measures are needed. Implantable valves are the final option, since they require surgery, are expensive, are molest because of their size and their conduits get obstructed frequently. Finally, as the disease follows its natural course, the amount of liquid to be drained increases. [1][2][3] [8][9][10].

Thus, there is a need of valves allowing large, variable actuator displacement and, as a consequence, permitting big molecules to pass through the valve without risk of obstruction, and providing variable hydraulic impedance. Large displacements in the actuator involve the use of big amounts of energy that can only be provided by active systems. Active systems require an energy source and extra blocks, which can be translated to bigger size and complexity for the valve. This might explain why available glaucoma valves remain passive.

To serve these problems an active valve is proposed using MEMS technology. The nano and microscale size of the components will allow the addition of the extra blocks needed for the active system, which will deliver the energy that the actuator needs. An external power source will provide the energy via a 13.56MHz inductive coupling. A DBS-PPY electrochemical diaphragm fed by a potentiostat, will be used as an actuator. An application specific integrated circuit (IC), will condition

the signal induced in the internal coil to power the potensiostat, and provide for the reference voltage. This reference will vary according to the required actuation level, and will be proportional to the duty cycle of the 13.56MHz amplitude modulated signal.
Other implants have already used the idea of including an IC and a telemetric link. Well known examples are pacemakers. In addition, other implantable devices have already implemented the usage of wireless power supplies. Such is the case of cochlear implants, devices for health information and patient identification, and retinal implants. However, there are no reports about a wirelessly powered active ocular implant for the treatment of glaucoma. [4] [5] [6] [7].
In this paper a testing circuit, called discrete transponder (TPD) is proposed, implemented and characterized. The TPD emulates the behavior of the IC, thus allowing the improvement of its design and, above all things, the characterization of the actuator and the RF link. Finally, it will provide the first information about the overall performance of the system.

2. Generation of the RF stimulation signal

The RF stimulation signal should have the characteristics listed in Table 1

Table 1. RF stimulation signal desired parameters.

Parameter	Value	Unit
Carrier frequency	13.56	MHz
Modulation frequency	485	KHz
Modulation	ASK	
Modulation Index (MI)	>30	%
Power	400	mW
Working cycle resolution	3.57	%

In order to generate the RF stimulation signal, an evaluation board provided by Texas Instruments, more precisely a TRF7960AEVM, was modified. The firmware of the module was rewritten in order to meet the features named in Table 1.

3. Design and implementation

3.1. Requirements for the TPD

The TPD should provide a means for testing PPY-DBS electrochemical actuators. So as to be able to fix the excitation voltage, a potentiostat should be used. In order to provide full electrical characterization of the actuator, a means for measuring the current delivered to the electrochemical cell´s working electrode should be included. Furthermore, the TPD should receive wirelessly information about the level of actuation. In order to avoid a high power RF source, the TPD must be fed by a source other than the RF power.
The supply block of the TPD should receive at least ±6V and provide the rest of the circuit with ±5V regulated. In order to stimulate the potentiostat, the TPD should generate a reference voltage proportional to the RF signal working cycle. This reference should be in the ±1V range, as higher voltages may damage the actuator.

3.2. TPD Blocks

To meet the requirements previously presented, the following blocks were considered for the TPD circuit.

3.2.1. RF acquisition. Comprising a tank circuit tuned to 13.56 MHz, and adapted to the impedance of the rectification block.

3.2.2. RF rectification, filtering and offset removal. The purpose of these blocks is to filter the carrier and to obtain the modulated signal. To achieve this, a diode bridge and a first order lowpass filter with cutoff at 1 MHz, was used.

3.2.3. Range correction. The amplitude of the induced signal depends on variables such as the distance and coil alignment. In order to fix the range to a known value, a transistor working in its cutoff and saturation regions was used.

3.2.4. Reference voltage generation. So as to obtain a voltage propotional to the RF signal working ratio (V_{ref}), a second order lowpass filter with cutoff at 66.6 Hz, was used. An offset correction stage was also included in this block.

3.2.5. Potentiostat. A potentiostat maintains the voltage between the working (WE) and the reference electrodes (RE) of an electrochemical cell, to a fixed reference value. This reference is provided by the previous block.

3.2.6. Working electrode current measurement. In order to measure this current, a transimpedance amplifier connected the WE was used.

3.2.7. Power supply. This block, generates ±5V required by the active blocks.

A block diagram of the circuit is shown in figure 1, where all the blocks were identified.

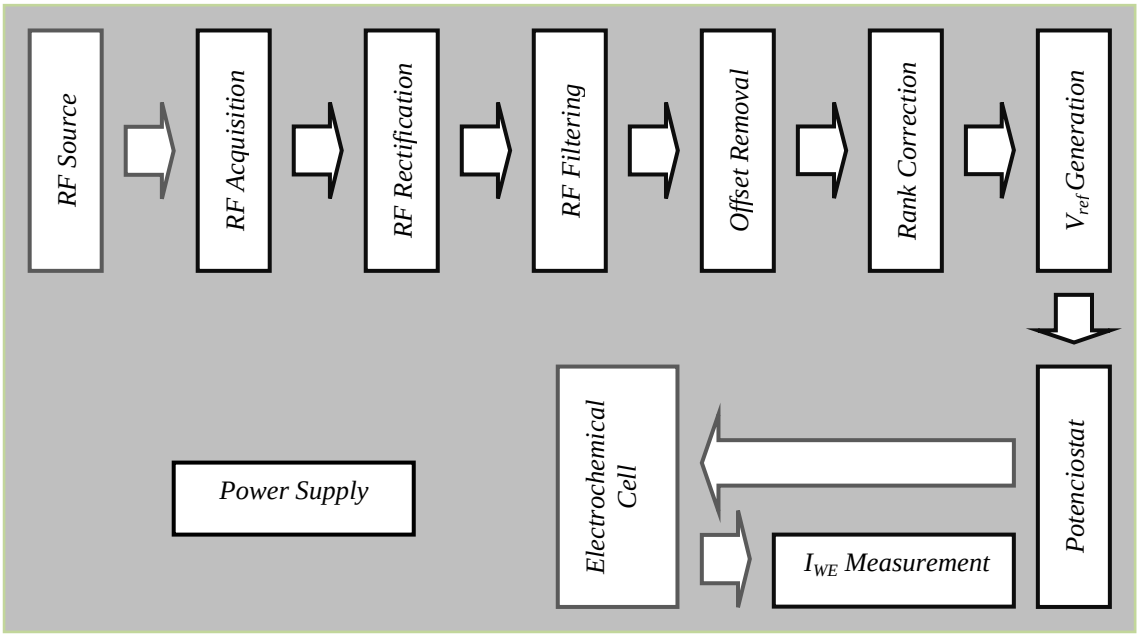

Figure 1. Block diagram for the TPD.

4. Characterization

To evaluate the behavior of the circuit when exposed to a RF stimulation signal, several test were performed. All the informed voltages are measured with respect to ground.

4.1. RF source characterization

The TRF7960AEVM module (the RF source) was characterized as regards to carrier and modulation frequency, IM and WC using an Instek GDS-806C oscilloscope. The setup used, is shown in figure 2. All different possible WC were set, and on and off times were measured. Figure 3 shows the waveform obtained for a WC = 75 %. Table 2 shows the measured values of the RF signal, and table 3 shows the calculated WC values.

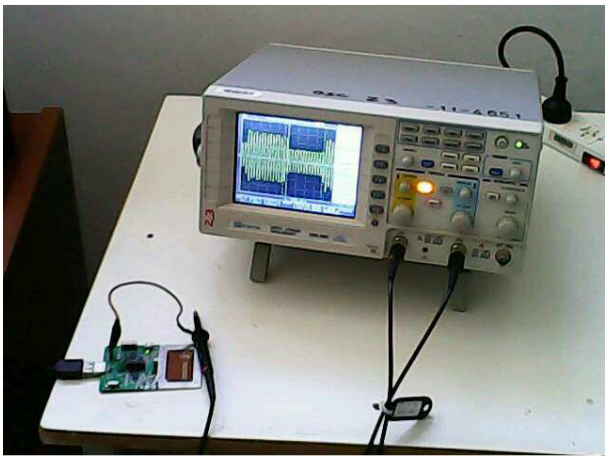

Figure 2. Laboratory Setup for experience 4.1.

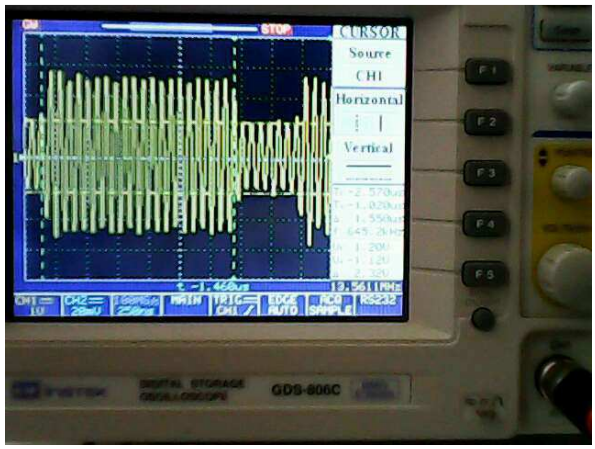

Figure 3. RF excitation signal with WC = 75%.

Table 2. RF excitation signal measured parameters.

Parameter	Value	Unit
Carrier frequency	13.5611	MHz
Modulation frequency	482.85	KHz
Modulation Index (MI)	45	%

Table 3. RF excitation signal measured parameters.

Theoretical WC (%)	T_{on} (ns)	T_{off} (ns)	T_{total} (ns)	Measured WC (%)	Error (%)
0	0	2065	2065	0	0
35.71	720	1360	2080	34.6153846	1.09461538
39.28	810	1250	2060	39.3203883	0.04038835
42.86	890	1190	2080	42.7884615	0.07153846
46.42	1031	1110	2141	48.1550677	1.73506773
50	1040	1030	2070	50.2415459	0.24154589
53.57	1110	960	2070	53.6231884	0.05318841
57.14	1190	880	2070	57.4879227	0.34792271

4.2. Induced amplitude vs. distance

Amplitude of the induced voltage was obtained for several distances between the RF source and the TPD. For this purpose, the TRF7960AEVM connected to a PC, an Atten ADS1102CAL oscilloscope, two graving arms, and a ±12V power source, were used. This setup can be seen in figure 4. WC of the RF excitation signal was set to 50%.

Figure 4. Setup for RF experience 4.2.

The measure was not performed in the tank circuit, because the oscilloscope probe capacitance would have tuned the circuit to another frequency. In return, the voltage in the RF Filtering block was measured. High and low levels of the square wave obtained in this block (the modulation signal) are plotted in figure 5 for different distances.

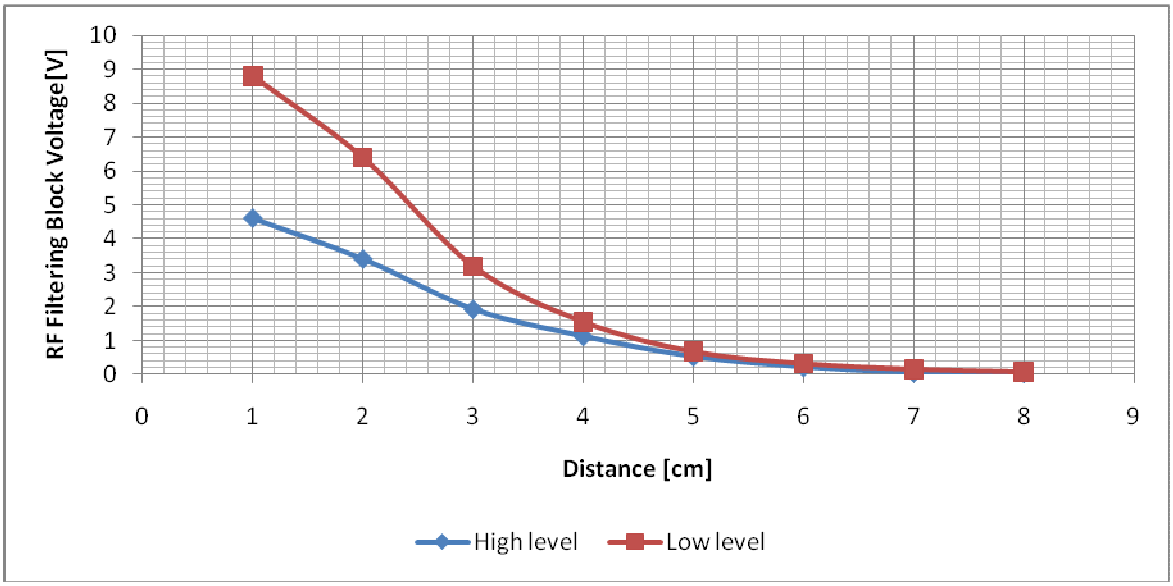

Figure 5. High and low levels in the RF Filtering block vs. distance between the RF source, and TPD.

4.3. Induced amplitude vs. coupling angle

The induced amplitude was obtained for several coupling angles. These, were measured between the projections of the coils planes. Setup used was similar to the one used in 4.2. The distance between the center of the coils of RF source and TPD, was equal to 4 cm. Results are shown in fig. 6.

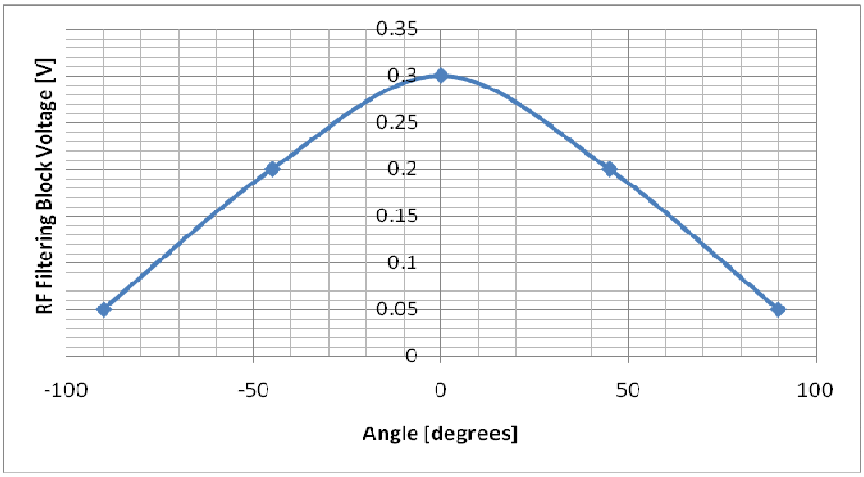

Figure 6. High level in the RF filtering block vs. angle between the RF source and TPD.

4.4. Range correction vs. distance

The voltage amplitude in the range correction block was obtained for several distances between the RF source and the TPD. Setup used was identical to the one in 4.2. Results are shown in fig. 7.

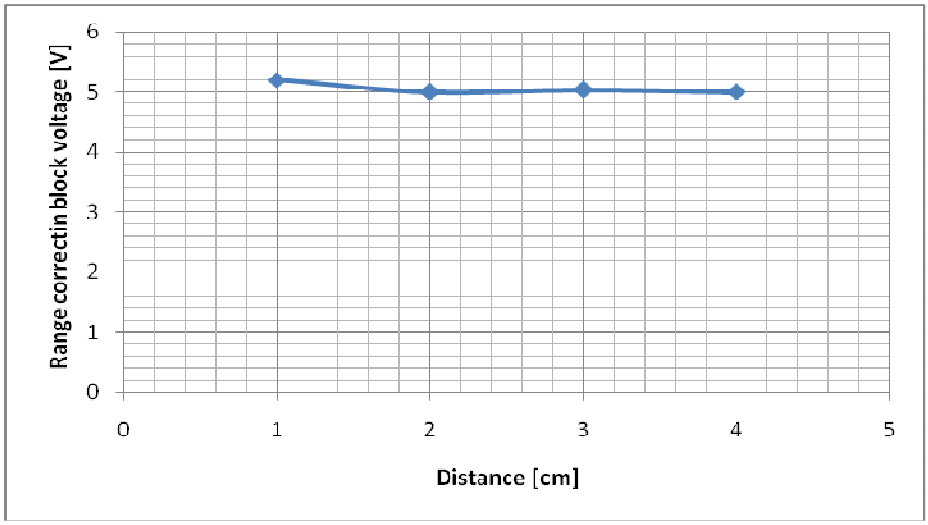

Figure 7. High level in the range correction block vs. distance between the RF source and TPD.

It has to be noted that the waveform obtained at this instance was not perfectly square, and changed with distance.

4.5. TPD WC vs. RF source WC

Using a setup similar to 4.2, but keeping the distance between the RF source and the TPD fixed to 2 cm, WC in the Range correction block of the TPD was measured for each possible WC of the RF source. In figure 8, results can be seen.

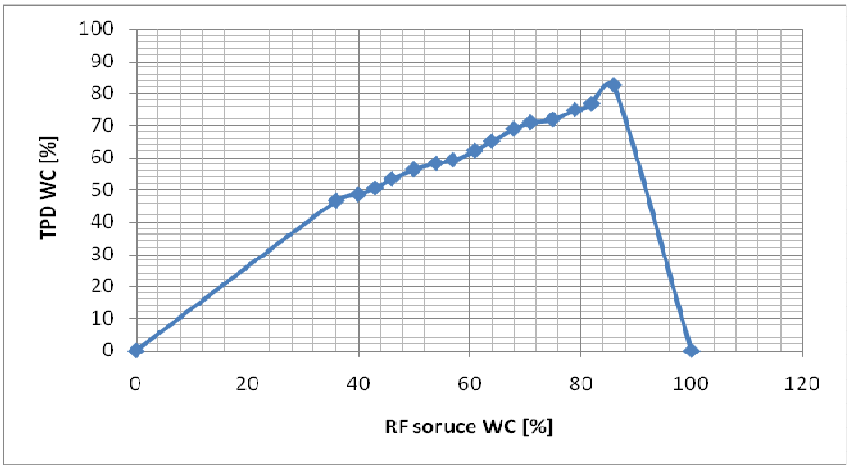

Figure 8. TPD WC vs. RF source WC.

4.6. V_{ref} vs. distance

V_{ref} was measured for several distances between the RF source and the TPD. Setup used was identical to the one in 4.2. Results are shown in figure 9.

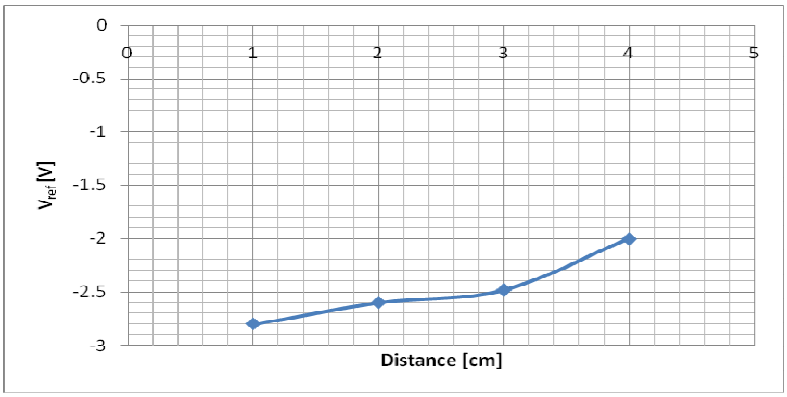

Figure 9. V_{ref} level vs. distance between the RF source and TPD.

4.7. V_{ref} vs. distance

V_{ref} was measured for all the possible values of WC. Setup used was identical to the one in 4.5 and results are shown in figure 10.

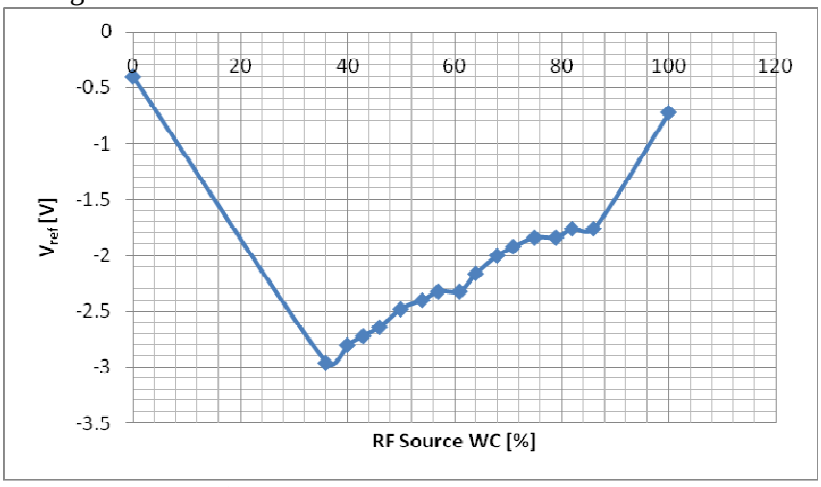

Figure 10. V_{ref} vs. RF source WC.

5. Discussion

The RF source modulation index, carrier and modulation frequencies took design values given in table 1. Perceptual error between software set working cycle, and measured working cycle was minor to 2% in all cases.

Test 4.2, showed typical $1/r^2$ decay in induced voltage, as distance increased. Test 4.3 showed that maximum coupling occurred when coils were parallel, and no coupling at all was found when angle between planes was 90°. This is logical since in the center of the RF source coil, magnetic flux is normal to it. This means that no flux will pass through the TPD coil when the angle is 90° and no voltage will be induced according to Faraday's Law. In the other hand, the contrary situation (parallel coils) will cause maximum induction.

Range correction block, was characterized in test 4.4. Although the waveform high level value was the expected, the shape was not perfectly square and changed with distance. This phenomenon had repercussions in test 4.6, where V_{ref} varied with distance even though it was expected no to.

Figures 8 and 10, show that V_{ref} and TPD WC change lineally with RF source WC except when WC = 0 and 100%. The reason is that a pure 13.56 MHz excitation signal, will not pass the RF Filtering block. If these values for WC are removed, linearity becomes evident (see fig. 11 and 12). In fact, R^2 parameters remain close to the unity in both cases.

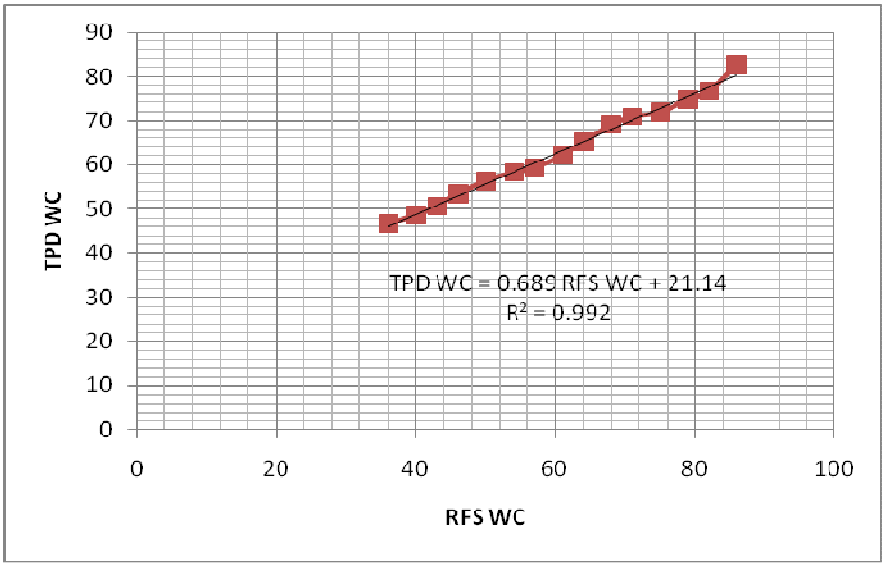

Figure 11. TPD WC vs. RF source WC (0 and 100% not considered).

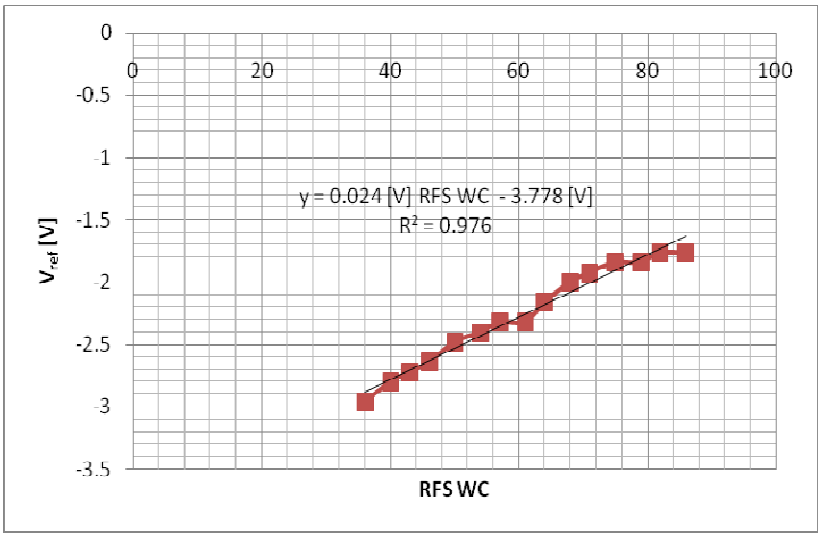

Figure 12. V_{ref} vs. RF source WC (0 and 100% not considered).

6. Conclusions

TRF7960AEVM behaved as expected regarding to MI, carrier frequency, modulation frequency and working cycle. The output power remains to be characterized.

Tests 4.2 to 4.7 were designed to test the RF link. TPD responses were the expected with two exceptions. First, a distance variation between the RF source and the TPD produced a V_{ref} variation. This undesired phenomenon may be solved by causing the transistor in the range correction block to enter saturation more easily, and thus obtaining square waveforms. A Darlington configuration should be considered in a future version. Second, working cycles of 0% and 100% will produce non linearities in V_{ref} vs. WC plot. This can be easily solved by not using those values for WC. Leaving those issues aside, the RF coupling performed properly. In order to achieve the desired potentiostat output, the offset correction stage should add 1.89 V to V_{ref}, so that plot at figure 12 is centered at 0 V. Amendment of these problems, potentiostat characterization, and actuation of PPY-DBS electrochemical cells wirelessly are left for future research.

References

[1] Quigley H A 1996 Number of people with glaucoma worldwide *Br J Ophthalmol* **80(5)** 389-393.

[2] Alañón Fernández F J, Fernández Pérez J, Ferreiro López S 2003 Oftalmología En Atención Primaria *Formación Alcalá.*

[3] Huang M C, Netland P A, Coleman A L, Siegner S W, Moster M R and Hill R A 1999 Intermediate-term clinical experience with the Ahmed Glaucoma Valve implant *A J Ophthalmol* **127(1)** 27-33.

[4] Ashar B S and Ferriter A 2007 Radiofrequency Identification Technology in Health CareBenefits and Potential Risks *JAMA* **298(19)** 2305-2307

[5] Michael K and Masters A 2004 Applications of human transponder implants in mobile commerce *Proceedings of the 8th World Multiconference on Systemics, Cybernetics and Informatics* **5** 505-512

[6] Roessler G, Laube T, Brockmann C, Kirschkamp T, Mazinani B, Goertz M, Koch C, Krisch I, Sellhaus B, Trieu HK, Weis J, Bornfeld N, Röthgen H, Messner A, Mokwa W and Walter P. 2009 Implantation and Explantation of a Wireless Epiretinal Retina Implant Device: Observations during the EPIRET3 Prospective Clinical Trial *Invest Ophthalmol Vis Sci. 50(6)* 3003-8

[7] Moctezuma A, Tu J 2011 An Overview of Cochlear Implant System

[8] Beck A D, Freedman S, Kammer J and Jin J 2003 Aqueous shunt devices compared with trabeculectomy with Mitomycin-C for children in the first two years of life *American Journal of Ophthalmology*, **136**(6) 994–1000.
[9] Hau S and Barton K 2009 Corneal complications of glaucoma surgery *Current Opinion in Ophthalmology* **20(2)** 131- 136
[10] Minckler D S, Francis B A, Hodapp E A, Jampel H D, Lin S C, Samples J R, Smith S D and Singh K 2008 Aqueous Shunts in Glaucoma: A Report by the American Academy of Ophthalmology *Ophthalmology* **115(6)** 1089–1098